ENERGY TRANSFER BETWEEN POD MODES OF FORCED TURBULENT FLOW OVER A FENCE

Alexander Orellano *, Jens Neumann and Hans Wengle †
Institut für Strömungsmechanik und Aerodynamik, LRT/WE7
Universität der Bundeswehr München, D-85577 Neubiberg, Germany

ABSTRACT

From large-eddy simulations of unforced and forced turbulent boundary layer flow over a surface-mounted fence of height h (Re_h = 3000) samples in time have been collected. These samples (snapshots) of the flow field have been used to carry out three-dimensional proper orthogonal decompositions (POD), in order to extract the dominating spatio-temporal structures of the flow.

The energy balance equation for an individual mode can be derived using a Galerkin projection of the Navier Stokes equation onto the POD modes. These POD modes have also been utilized to evaluate the nonlinear energy transfer terms. It can be concluded that the (high-frequency) roll-up process in the separated shear layer receives most of the energy from the mean flow and exchanges little energy with the other modes. In comparison to this, the (low-frequency) shedding of large-scale structures from the recirculation bubble receives larger amounts of energy from the mean flow and in addition, exchanges one order of magnitude larger amounts of energy with the 'neighbouring' modes. This also explains why, in our flow case, the low-frequency forcing (with $Str = 0.08$) leads to a much stronger reduction of the mean re-attachment length (36%) than the high-frequency forcing (with $Str = 0.60$).

INTRODUCTION

We investigated forced turbulent boundary layer flow over a surface-mounted fence, for a Reynolds number of Re_h = 3000 (based on fence height, h, and maximum inflow velocity, U_∞). The flow has been manipulated by time-periodic blowing/suction forcing (with a forcing amplitude $w_{forcing}/U_\infty = 0.5$) through a narrow slot upstream of the obstacle, see *figure 1*, and in Orellano and Wengle (2000).

*present address: ADtranz Regional Trains, Am Rathenaupark, D-16761 Hennigsdorf, Germany
†Contact by e-mail: hans.wengle@unibw-muenchen.de

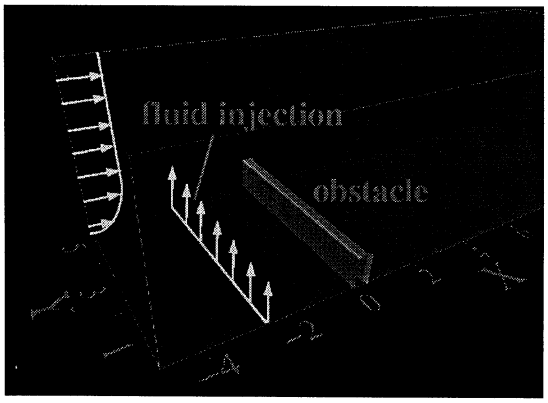

Figure 1: Computational domain (with forcing slot at X=-3)

In addition to the unforced reference case, two manipulated flow cases were numerically simulated by Large-Eddy Simulation (LES): a first case with high-frequency forcing ($Str_1 = f_1 h/U_\infty = 0.60$) which leads to about 10% reduction of the mean re-attachment length, x_r/h, and a second case with low-frequency forcing ($Str_2 = f_2 h/U_\infty = 0.08$) which resulted in a 36% reduction of x_r/h. Details of the results can be found in Orellano and Wengle (2000). In the low-frequency forced case, large two-dimensional structures are created already in front of the flow obstacle. They roll over the fence (nearly unaffected by the flow obstacle) and, after the fence, they fill the entire height of the recirculation bubble, rolling downstream and thereby entraining a lot of fluid material from outside. This striking feature created the motivation to continue this work with the objectives
(a) to analyse the flows by a Karhunen-Loève expansion, also called "Proper Orthogonal Decomposition" (POD), and
(b) to apply a Galerkin projection of the Navier-Stokes equation onto these POD modes to identify and evaluate the energy transfers which are involed in the energy budget of an individual mode.

POD OF THE FLOW FIELD

For the PODs we used data sets from about 174000 grid points from the LES (with about 1.67 million grid points) within a subdomain of the computational domain. This subdomain included parts of the incoming turbulent boundary layer, the complete separated flow region in front of the fence and the separated shear layer bounding the long separation zone after the flow obstacle.

A rapidly converging representation of the velocity field can be expressed using spatial functions $\phi_i^n(\vec{x})$ together with temporal coefficients $a^n(t)$:

$$u_i(\vec{x},t) = \sum_{n=1}^{N_M} a^n(t)\phi_i^n(\vec{x}) \quad . \qquad (1)$$

In the application of the POD used here we followed the treatment proposed by Sirovich (1987) ("method of snapshots") and Aubry (1991) ("bi-orthogonal decomposition"), see also in Manhart and Wengle (1993). Here, we used 6000 samples (snap shots) for each analysis. The method of snapshots leads to an eigenvalue problem with the temporal autocorrelation C(t,t') as the kernel:

$$\int_T C(t,t')a^n(t')dt' = \lambda^n a^n(t) \qquad (2)$$

In this case, C(t,t') must be evaluated from

$$C(t,t') = \frac{1}{T}\int\int\int_V u_i(\vec{x},t)u_i(\vec{x},t')d\vec{x} \qquad (3)$$

and the spatial modes, $\phi_i^n(\vec{x})$, can be calculuated from

$$\phi_i^n(\vec{x}) = \frac{1}{T}(\lambda^n)^{-1}\int_T a^n(t)u_i(\vec{x},t)dt \qquad (4)$$

Eigenvalues.

The time-averaged energy content of a Karhunen-Loève mode with mode number n is represented by the corresponding eigenvalue, λ^n. The sum of all the eigenvalues is equal to the total kinetic energy of the flow field or, excluding mode n=1, equal to the turbulent energy of the flow. Note, for the evaluation presented in this paper, the total velocity (not the fluctuating part only) has been analysed. Then, in a statistically stationary flow, the first mode represents the time-averaged flow.

Figure 2 shows the distribution of the eigenvalues over the mode number, n, for the three flow cases. It is interesting to observe that, in our flow case, about the first fourty eigenvalues for the fluctuating flow field (n=2 to 41) decay very slowly from about 1.0 to 0.1, for the reference case $f03_{aa}$ (Str=0) and for the high-frequency forced case $f03_{ad}$ (Str=0.60). However, in the the low-frequency forced case $f03_{af}$ (Str=0.08) the first two fluctuating modes (n=2 and 3) are acting as dominating modes with significantly larger energy content in comparison to the other modes.

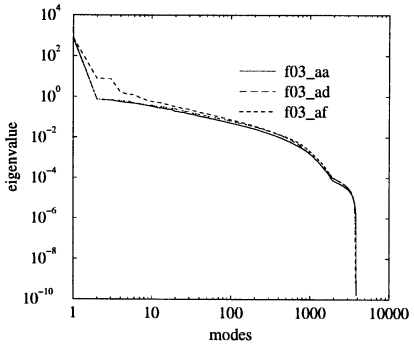

Figure 2: Eigenvalue spectra of the POD modes for the reference case $f03_{aa}$, and for the forced cases, $f03_{ad}$ (Str=0.6) and $f03_{af}$ (Str=0.08).

The accumulated energy ratio, $e_r(k)$, of the fluctuating POD modes ($k = n - 1$) can be evaluated from

$$e_r(k) = \frac{\sum_k \lambda(k)}{\sum_{NM} \lambda(k)}. \qquad (5)$$

and *figure 3* shows $e_r(k)$ for the three flow cases. About 2000 POD modes are required to represent about 99% of the turbulent kinetic energy. In equation (5) above, N_M is the number of positive non-zero eigenvalues, which gives a measure for the dimension of the system of orthogonal modes (the so-called Karhunen-Loève dimension). The first 20 modes represent about 25% of the turbulent kinetic energy for the reference case and for the high-frequency forced case, and about 50 % for the low-frequency forced case.

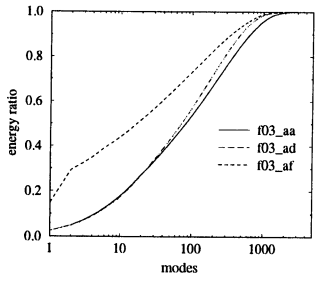

Figure 3: Accumulated energy ratio $e_r(k)$ for the reference case $f03_{aa}$, and for the forced cases, $f03_{ad}$ (Str=0.6) and $f03_{af}$ (Str=0.08).

The high-frequency forced case (Str=0.6).

The forcing frequency (Str=0.60) used in this case is the sub-harmonic of the primary roll-up of the shear layer (Str=1.2). Here, the first 20 eigenvalues are close together, and mode pairs do not necessarily appear with two successive mode numbers. Therefore, the spatial and temporal mode pairs representing the roll-up process are connected with the mode numbers n=3 and n=16, see *figure 4* and *figure 5*. The phase shifts between the two spatial and corresponding temporal modes lead to a downstream travelling wave. However, the roll-up process of the separated turbulent shear layer seems to be settled at a downstream distance of about five fence heights. Therefore, using a shorter volume of interest for the POD will result in relatively larger energy content of this roll-up process and indeed, in Orellano and Wengle (1999) it has been represented by the mode pair 2/3 (even with a much smaller number of snapshots).

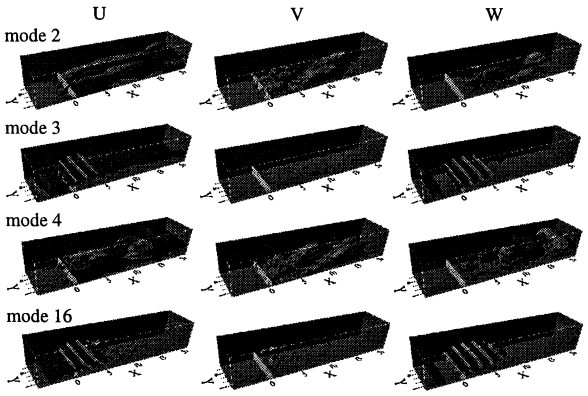

Figure 4: Spatial modes of case $f03_{ad}$ ($Str = 0.6$)

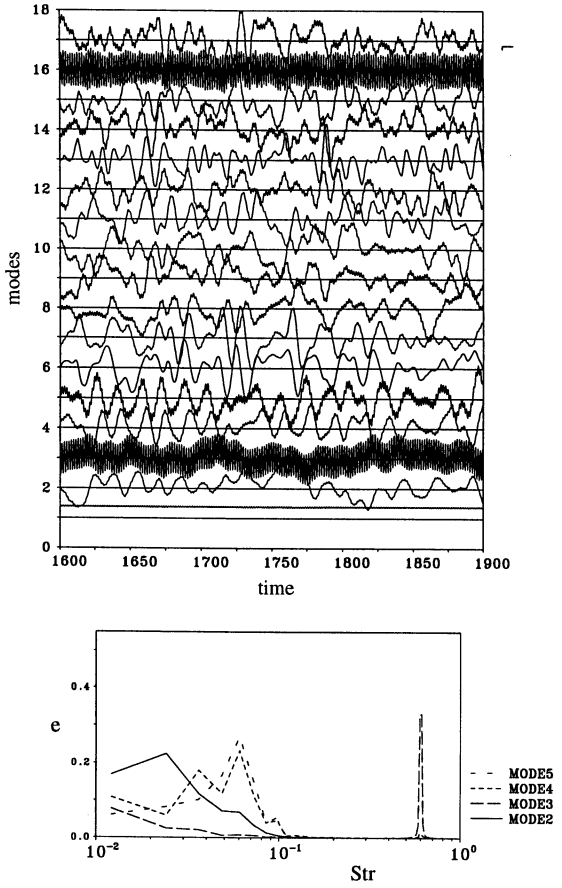

Figure 5: Temporal coefficients $a^n(t)$ (above) and energy spectra (below) of selected $a^n(t)$ of the high-frequency forced case (Str=0.60)

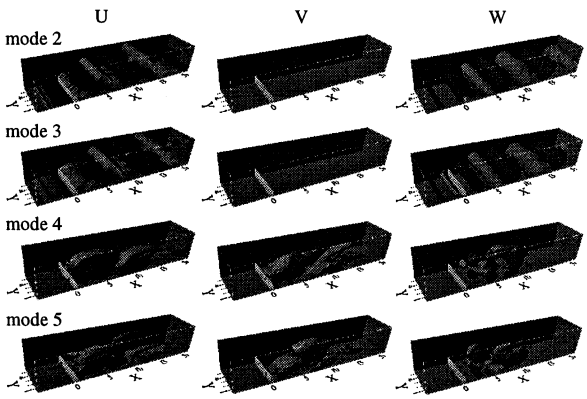

Figure 6: Spatial modes of case $f03_{af}$ ($Str = 0.08$)

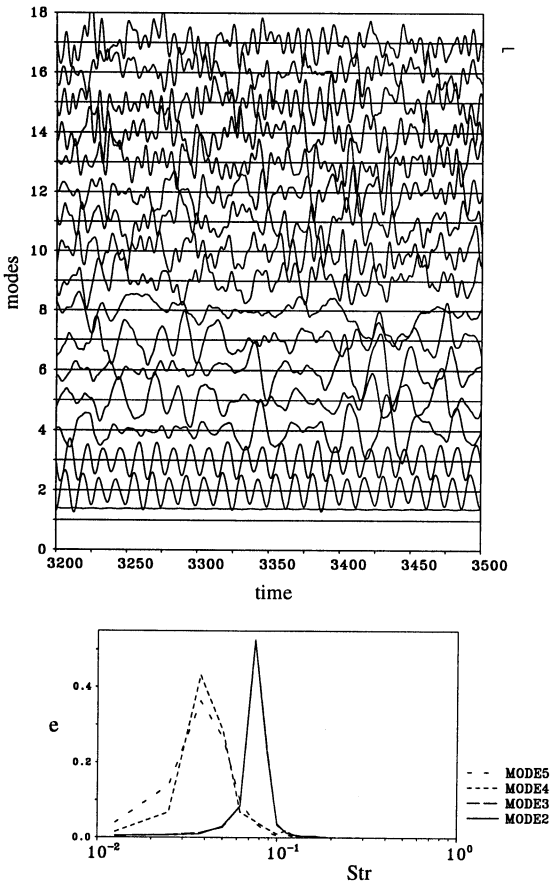

Figure 7: Temporal coefficients $a^n(t)$ (above) and energy spectra (below) of selected $a^n(t)$ of the low-frequency forced case (Str=0.08)

Figure 5 (above) shows the temporal modes, $a^n(t)$. From a Fourier analysis of the first few temporal modes (*figure 5* (below)) it can be seen that most of the energy of the forcing mode n=3 (and also of mode n=16, not shown here) is related to the forcing frequency (Str=0.60). Low-frequency peaks can be observed at Str=0.08 for the mode pair n=4/5. This mode pair can again be identified with the ejection of large-scale structures from the recirculation bubble. Mode 2 reflects the low-frequency processes already amplified upstream of the fence (see details in Orellano and Wengle, 2000).

The low-frequency forced case(Str=0.08).

In this flow case the spatial mode pair 2/3 represents the low-frequency forcing mode which dominates the entire flow field, see *figure 6* and *figure 7*. The mode pairs n=4/5 and 6/7 represent *'subharmonic'* coherent structures in the sense that they are connencted with the subharmonic Strouhal number Str=0.045. There are also *'harmonic'* coherent structures to be detected in the flow field (e.g. n=13/14, not shown here).

The corresponding temporal modes in *figure 7* (above) also show the mode pairs mentioned above. A Fourier analysis of the first four fluctuating modes (n=2 to 5) displays for the forcing mode pair 2/3 a peak at Str=0.08 and for the subharmonic of this forcing mode a peak at Str=0.04, see *figure 7* (below).

It should be noted here again that in the forced flow cases the mode n=1 represents the mean flow. From a closer inspection of the temporal mode n=1 in *figure 5* and *figure 7* it can be realized that these mean flow modes are not exactly constant in time but also oscillate with the corrresponding forcing frequency. The forcing frequency also seems to be superimposed onto nearly all the other temporal modes with higher mode numbers.

GALERKIN PROJECTION OF THE NAVIER-STOKES EQUATION AND ENERGY TRANSFERS BETWEEN THE MODES

Substituting the velocity components, $u_i(\vec{x},t)$ (i=1,2,3), in the Navier-Stokes equations by their corresponding Karhunen-Loève expansion (temporal modes $a^k(t)$ and spatial modes $\phi_i^k(\vec{x})$) and carrying out a Galerkin projection of the Navier-Stokes equation onto the POD modes leads to the momentum balance of an individual mode k. From this, the mean energy budget of such an individual mode k can be derived:

$$\begin{aligned} < \frac{de^k}{dt} > &= \sum_l \sum_m n_{klm} < a^k a^l a^m > \\ &\quad + < a^k \hat{\pi}_k > \\ &\quad + \sum_l d_{kl} < a^k a^l > \\ &= T_k + P_k + D_k \end{aligned} \tag{6}$$

Here, the third and the second term on the right hand side represent the diffusive interactions and the interactions with the pressure field, respectively. In this paper, we are interested in particular in the first term on the right hand side of (6) representing the non-linear energy transfer between mode k (which receives energy) and the mode l (which provides energy) with the aid of a transport mode m (which acts as a bridge over which the energy is transferred), see, e.g. in Manhart (1996,1999) and Orellano (1999). Taking into account the effect of *all* transport modes, m, leads to the mean energy flux, Q_{kl}, from mode l to mode k:

$$Q_{kl} = \sum_m n_{klm} < a^k a^l a^m > \tag{7}$$

We are also interested in the mean energy flux from the mean flow (mode l=1) to an individual mode k:

$$Q_{k1} = \sum_m n_{k1m} < a^k a^1 a^m > \tag{8}$$

As a typical example from our analysis, *figure 8* presents the numerically evaluated fluxes, Q_{k1}, from the mean flow (mode l=1) to the individual modes (k=2,3, ...). It is obvious from this figure that in the low-frequency forcing case (Str=0.08) these energy fluxes to the first six (fluctuating) modes are significantly stronger in comparison to the high-frequency forced case (Str=0.60).

Figure 9 gives a first explanation for the totally different behaviour of the low-frequency forced case: in comparison to the high-frequency forced case (and in comparison to the unforced case, not shown here) large amounts of energy are transferred between modes with relatively low mode numbers only.

Finally, *figure 10* compares the individual energy fluxes between the forcing modes and the other modes. In the low-frequency forced

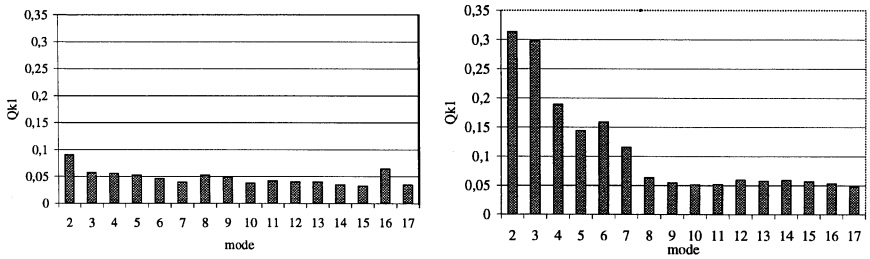

Figure 8: Mean energy flux, Q_{k1}, from the mean flow (l=1) to an individual mode k
left: high-frequency forced case (Str=0.60), right: low-frequency forced case (Str=0.08).

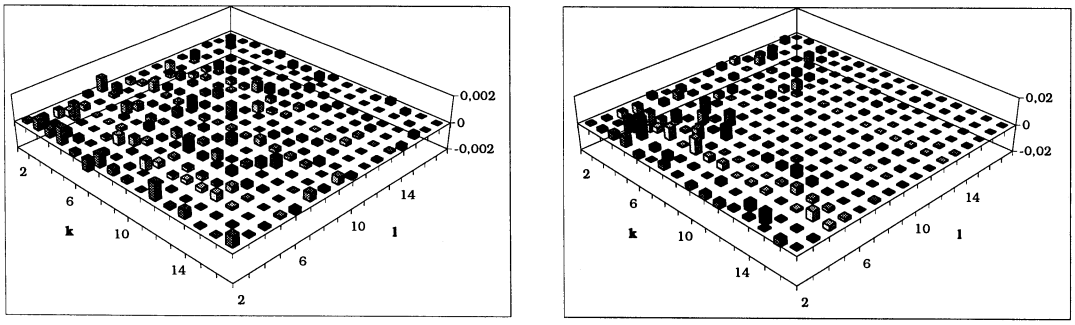

Figure 9: Mean energy flux, Q_{kl}, between mode l and mode k
left: high-frequency forced case (Str=0.60), right: low-frequency forced case (Str=0.08).

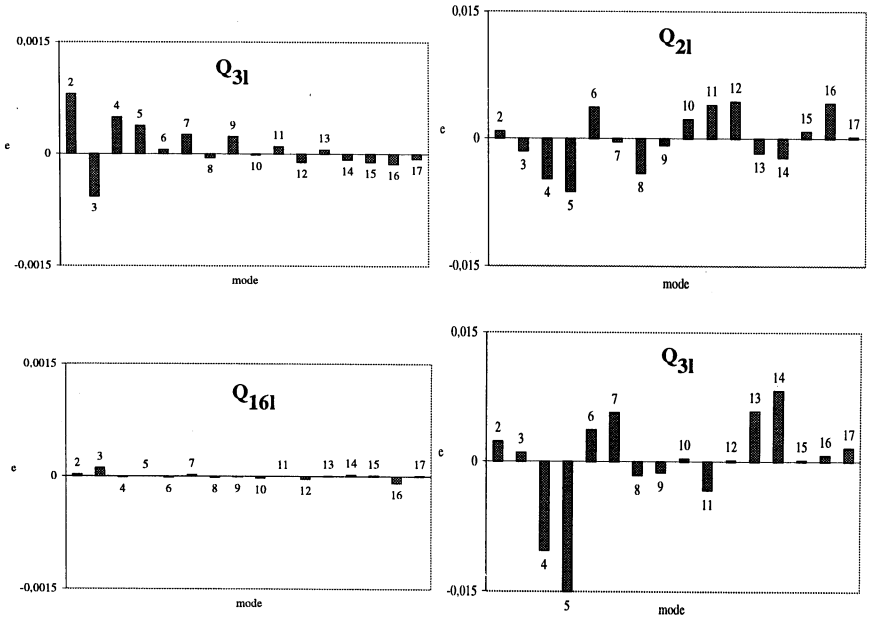

Figure 10: Individual mean energy fluxes between the forcing modes and the other modes l
left: high-frequency forced case (Str=0.60), with forcing mode pair (k=3 and 16),
right: low-frequency forced case (Str=0.08), with forcing mode pair (k=2 and 3)
Note, the ordinate of the figures on the right hand side is one order of magnitude larger than on the left hand side.

case the energy fluxes to the neighbouring modes are about one order of magnitude larger than in the high-frequency forced case. Note the different scaling of the ordinate in *figure 10*(left) and *figure 10*(right).

CONCLUSIONS

The fully three-dimensional eigenmode decomposition of the flow fields in a large domain of interest (enclosing the separation zone in front of the fence, the total recirculation zone after the fence, and a region beyond the location of mean re-attachment) reveals the major dynamic processes in the flow, such as the roll-up of the turbulent shear layer and the shedding of large-scale structures from the recirculation bubble behind the flow obstacle. In the forced flow cases, corresponding forcing modes can be identified as pair of modes.

Due to the orthogonality of the spatio-temporal eigenmodes from POD, the energy transfers between individual modes (coherent structures) and from the mean flow (in our case represented by the first mode) can be calculated separately from the balance equation of the kinetic energy of an individual mode (utilizing a Galerkin projection of the Navier-Stokes equation onto these eigenmodes). The mean flow delivers energy to all the modes. However, in the low-frequency forced case the first five (most energetic) modes receive between 3 and 5 times as much energy in comparison to the other (less energetic) modes. Also in this case the non-linear activity between the modes is one order of magnitude larger in comparison to the other flow cases. In addition, the low-frequency forced case clearly demonstrates the non-linear energy transfer from 2D modes to 3D modes. With respect to the major dynamic processes in our flow case, it can be concluded that the roll-up process in the shear layer receives most of its energy from the mean flow and exchanges relatively little energy with the other modes. In comparison to this, the shedding of large-scale structures from the recirculation bubble receives larger amounts of energy from the mean flow and exchanges one order of magnitude larger amounts of energy with the 'neighbouring' modes. This also explains why, in our flow case, the low-frequency forcing (with $Str = 0.08$) leads to a much stronger reduction of the mean re-attachment length than forcing the shear layer roll-up (with its subharmonic $Str = 0.60$).

Acknowledgements

We are grateful to Dr. M. Manhart (Lehrstuhl für Fluidmechanik, Technical University of Munich) for many helpful discussions. This research was supported by the Deutsche Forschungsgemeinschaft (DFG) under grant number We 705/6&7. We also gratefully acknowledge the support by the Leibniz Computing Center (LRZ) of the Bavarian Academy of Sciences, and by the computing center of the Federal Armed Forces University Munich.

References

Aubry, N. (1991), "On the hidden beauty of the proper orthogonal decomposition", *Theoret. Comput. Fluid Dynamics*, 2, pp.339-352.

Manhart M. and Wengle H. (1993), "A spatiotemporal decomposition of a fully inhomogeneous turbulent flow field", *Theoret. and Comput. Fluid Dynamics*, 5, pp.223-242.

Manhart M. (1996), *"Umströmung einer Halbkugel in turbulenter Grenzschicht - Grobstruktursimulation und Eigenmodeanalyse der Ablöseprozesse"*, Fortschritt-Berichte VDI Reihe 7, Vol. 292, Dissertation (in german), Universität der Bundeswehr München. VDI-Verlag, Düsseldorf, 1996.

Manhart M. (1999), "Energy transfer between coherent structures in the wake of a hemisphere", IUTAM Symposium, 25-27 May 1997, Lyngby, Denmark, in *Simulation and Identification of Organized Structures in Flows*, pp.499-508, Berlin, Academic Publishers.

Orellano A. and Wengle H. (1999), "Visualization of coherent structures in manipulated turbulent flow over a fence", IUTAM Symposium, 25-27 May 1997, Lyngby, Denmark, in *Simulation and Identification of Organized Structures in Flows*, pp.15-24, Berlin, Academic Publishers.

Orellano, A. and Wengle H. (2000), "Numerical simulation (DNS and LES) of manipulated turbulent boundary layer flow over a surface-mounted fence",
Eur.J.Mech. B/Fluids 19 (5),pp 765-788.

Orellano A. (1999), *"Aktiv kontrollierte Hindernisumströmung in einer turbulenten Grenzschicht - Numerische Simulation einer Zaunüberströmung und Analyse der Wirbelstrukturen mittels einer Eigenmode-Zerlegung der Geschwindigkeiten"*, Fortschritt-Berichte VDI Reihe 7, Vol. 392, Dissertation (in german), Universität der Bundeswehr München. VDI-Verlag, Düsseldorf, 1999.

Sirovich L. (1987), "Turbulence and the dynamics of coherent structures", Part I,II,III, *Q. Appl. Math.*, 45(3), pp.561-590.